Copper complexes as biomimetic models of catechol oxidase: mechanistic studies

Koval, I.A.

8 | Catecholase activity of a copper(II) complex with the macrocyclic ligand [22]pr4pz: unraveling catalytic mechanisms[†]

In this chapter the structure, properties and a mechanism for the catecholase activity of a tetranuclear carbonato-bridged copper(II) cluster with the macrocyclic ligand [22]pr4pz (9,22-dipropyl-1,4,9,14,17,22,27,28,29,30-decaazapentacyclo-[22.2.1.1^{4,7}.1^{11,14}.1^{17,20}]triacontane-5,7(28),11(29),12,18,20(30),24(27),25-octaene) are reported. In this complex, two copper ions within a macrocyclic unit are bridged by a carbonate anion, which further connects two macrocyclic units together. The tetranuclear complex was found to be the major compound present in solution at high concentration levels, but its dissociation into two dinuclear units occurs upon dilution. The dinuclear complex catalyzes the oxidation of 3,5-di-*tert*-butylcatechol to the respective quinone in methanol by two different pathways, one proceeding via the formation of semiquinone species with the subsequent production of dihydrogen peroxide as a by-product, and another proceeding via the two-electron reduction of the dicopper(II) center by the substrate, with two molecules of quinone and one molecule of water generated per one catalytic cycle. The occurrence of the first pathway was, however, found to cease shortly after the beginning of the catalytic reaction. The influence of hydrogen peroxide and di-*tert*-butyl-*o*-benzoquinone on the catalytic mechanism has been investigated. The crystal structures of the free ligand and the reduced dicopper(I) complex, as well as the electrochemical properties of both the Cu^{II} and the Cu^{I} complexes are also reported.

[†]This chapter is based on: Koval, I. A.; Selmeczi, K.; Belle, C.; Philouze, C.; Saint-Aman, E.; Gautier-Luneau, I.; Schuitema, A. M.; van Vliet, M.; Gamez, P.; Roubeau, O.; Lüken, M.; Krebs, B.; Lutz, M.; Spek, A. L.; Pierre, J.–L.; Reedijk, J., Chem. Eur. J., submitted for publication

8.1 Introduction

In Chapter 7, the mechanism of catechol oxidation by a μ-hydroxo-dicopper(II) complex with the macrocyclic ligand [22]py4pz (Scheme 7.1, Chapter 7) has been discussed.[1] This dinucleating ligand provides two N_4 donor sets for the metal coordination. In the present chapter, the studies on the catecholase activity of the copper(II) complex with the related macrocyclic ligand [22]pr4pz (Figure 8.1) are presented. Instead of two pyridine-containing pendant arms, present in the ligand [22]py4pz, this ligand contains two propyl residues, thus providing two N_3 donor sets for the metal coordination, and mimicking the active site of the natural enzyme even more closely.

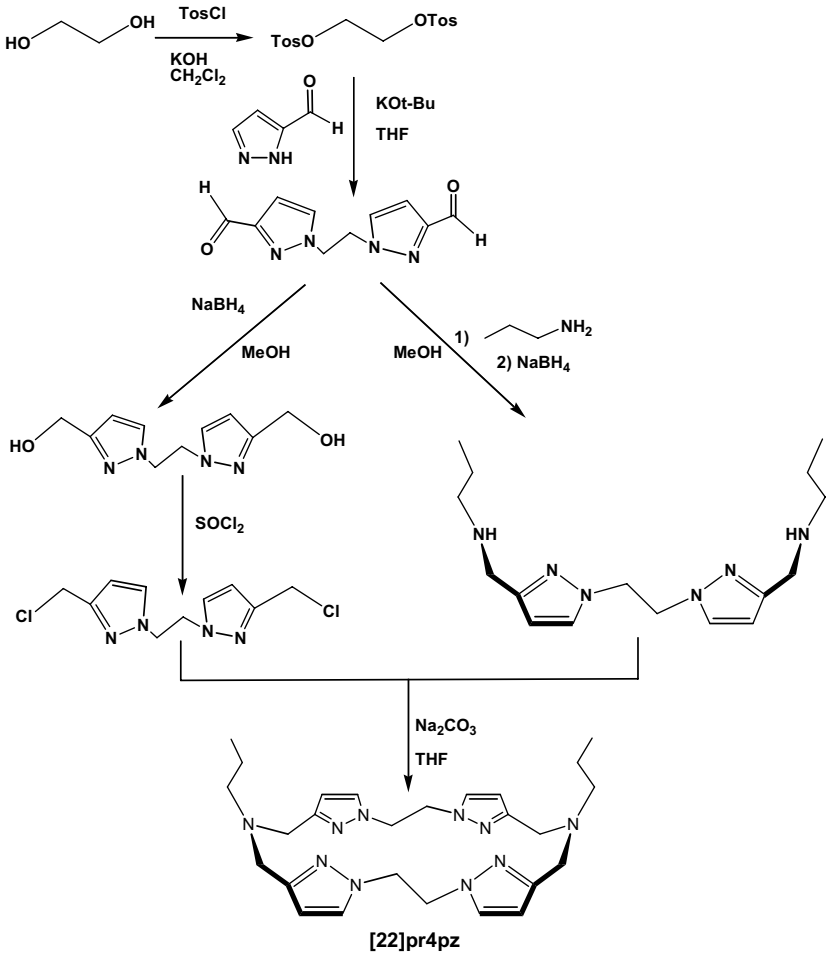

Figure 8.1. The reaction scheme of the synthesis of the macrocyclic ligand [22]pr4pz

In the isolated copper(II) complex with [22]pr4pz, the two metal ions within a macrocyclic unit are bridged by a carbonate anion, and two copper ions of two different macrocyclic units are further doubly bridged by two oxygen atoms of two carbonates, resulting in a tetranuclear structure in the solid state. In this chapter the crystal structures of the bis(perchlorate) salt of the macrocyclic ligand $[H_2[22]pr4pz](ClO_4)_2$,

the tetracopper(II) complex of the composition $[Cu_2([22]pr4pz)(CO_3)(H_2O)]_2(CF_3SO_3)_4 \cdot 2CH_3CN \cdot 4H_2O$ and its reduced dicopper(I) analogue $[Cu_2([22]pr4pz)(CH_3CN)_2](ClO_4)_2$, the kinetic studies on the catechol oxidation by the copper(II) complex and the anaerobic studies on its interaction with catechol are reported, and the catalytic reaction mechanism is discussed.

8.2 Results and Discussions

8.2.1 Synthesis of coordination compounds

The schematic representation of the synthesis of the macrocyclic ligand [22]pr4pz ((9,22-dipropyl-1,4,9,14,17,22,27,28,29,30-decaazapentacyclo-[22.2.1.$1^{4,7}$.$1^{11,14}$.$1^{17,20}$]triacontane-5,7(28),11(29),12,18,20(30),24(27),25-octaene) is depicted in Figure 8.1. This ligand has been designed earlier to model the active site of the structurally related type-3 copper protein hemocyanin.[2,3] The macrocyclic cavity comprises four pyrazolyl moieties and two nitrogen atoms of tertiary amine groups, providing two N_3 donor sets for the coordination of the metal ions. Diethyl ether diffusion in an acetonitrile solution, containing two molar equivalents of copper(II) triflate, one molar equivalent of the ligand and one molar equivalent of sodium carbonate, results in the formation of small blue crystals of the copper(II) complex. The X-ray structure determination (see below) revealed that it can be described as a tetranuclear complex of the formula $(\mathbf{1})_2(CF_3SO_3)_4 \cdot 2CH_3CN \cdot 4H_2O$, where $\mathbf{1}^{2+}$ corresponds to the dicopper unit $[Cu_2([22]pr4pz)(CO_3)(H_2O)]^{2+}$. The copper(I) complex was isolated by reacting two molar equivalents of Cu^I as a tetrakis(acetonitrile) complex with a solution of the ligand in methanol. The solid complex which precipitated upon addition of diethyl ether is the dinuclear Cu^I complex, denoted $\mathbf{2}(ClO_4)_2$, where $\mathbf{2}^{2+}$ corresponds to $[Cu_2([22]pr4pz)(CH_3CN)_2]^{2+}$.

8.2.2 Crystal structures description

$[H_2[22]pr4pz](ClO_4)_2$

An ORTEP projection of the bis(perchlorate) salt of the ligand is shown in Figure 8.2. The cationic ligand is located on an exact, crystallographic inversion center. The ligand adopts an *anti*-(chair) conformation, with two propyl groups located on opposite sides of the macrocyclic ring plane. Both symmetry-related tertiary amine nitrogen atoms (N27 and N27') are protonated, leading to a doubly charged cation, the positive charge being compensated by two perchlorate anions. The protonated N-H moiety acts as a donor of an intermolecular bifurcated hydrogen bond with two perchlorate oxygen atoms as acceptors; the angles at the hydrogen atom sum up to 359(4)° (Table 8.1). Due to the inversion center in the ligand the ring N21-N22 and its symmetry related N21'-N22' are arranged in a parallel fashion; the centroid-centroid

distance is 4.4089(18) Å and the parallel distance between the two planes of the aromatic rings is only 3.211 Å, indicating the presence of π stacking. The angle between the centroid-centroid vector and the normal to the aromatic ring plane is 43.25°.

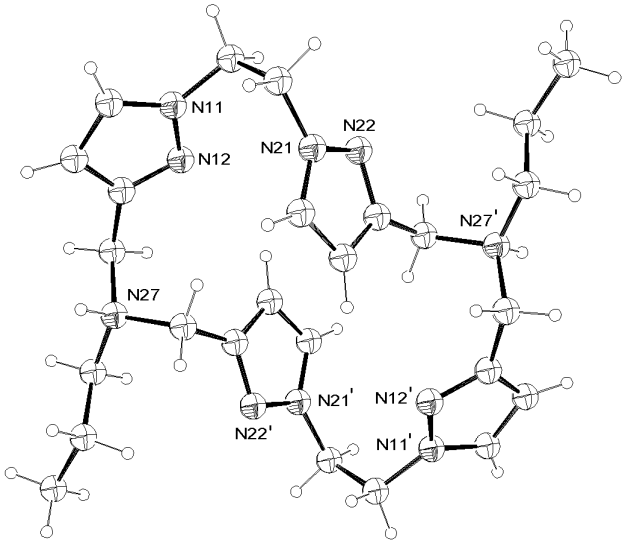

Figure 8.2. ORTEP projection of the cation $[H_2[22]pr4pz]^{2+}$. The perchlorate anions have been omitted for clarity. Symmetry operation ': 1-x, 1-y, 1-z.

Table 8.1. Bifurcated hydrogen bond for $[H_2[22]pr4pz](ClO_4)_2$

Donor - H....Acceptor	*D – H (Å)*	*H...A (Å)*	*D...A (Å)*	*D - H...A (°)*
N27 - H27…O3	0.92(3)	2.52(3)	3.233(3)	135(2)
N27 - H27...O3^{i}	0.92(3)	2.25(3)	3.063(3)	147(2)

Symmetry operation: i = 1-x, -y, 1-z; angle O1...H27...O1^{i}: 77.2(10)°

$[Cu_2([22]pr4pz)(CO_3)(H_2O)]_2(CF_3SO_3)_4 \cdot 2CH_3CN \cdot 4H_2O$

The molecular structure of the isolated solid complex consists of a tetracopper complex cation $[Cu_2([22]pr4pz)(CO_3)(H_2O)]_2^{4+}$ ($(\mathbf{1})_2^{4+}$), four counter ions $CF_3SO_3^-$, two non-coordinated acetonitrile molecules and four non-coordinated water molecules. An ORTEP projection of the structure of the cation $(\mathbf{1})_2^{4+}$ is shown in Figure 8.3 (top), selected bond lengths and angles are reported in Table 8.2. The cation contains four copper(II) centers, two macrocyclic ligands, two coordinated carbonates and two coordinated water molecules. In contrast to the structure of the protonated ligand, [22]pr4pz adopts a *syn*-(boat) conformation, with two propyl residues located on the same side of the macrocyclic ring plane. Each macrocyclic unit encloses two copper(II) ions (Cu1 and Cu2, and Cu1' and Cu2'), which are bridged by a carbonate anion (the Cu1…Cu2 or Cu1'…Cu2' intra-macrocyclic distance is 4.5427(18) Å). Two bridging oxygen atoms O51 and O51' from two different carbonate molecules connect the two central copper atoms Cu1 and Cu1' to form a centrosymmetric four-membered ring,

resulting in the Cu1…Cu1' inter-macrocyclic distance of 3.281(2) Å. Each carbonate ion is thus bound in a *syn, syn-anti* fashion, *e.g.* one of the oxygen atoms of the carbonate anion (O51 and O51') is bridging the coppers Cu1 and Cu1' of two different macrocyclic rings, whereas another oxygen atom (O52 and O52') binds to another copper ion (Cu2, Cu2' respectively).

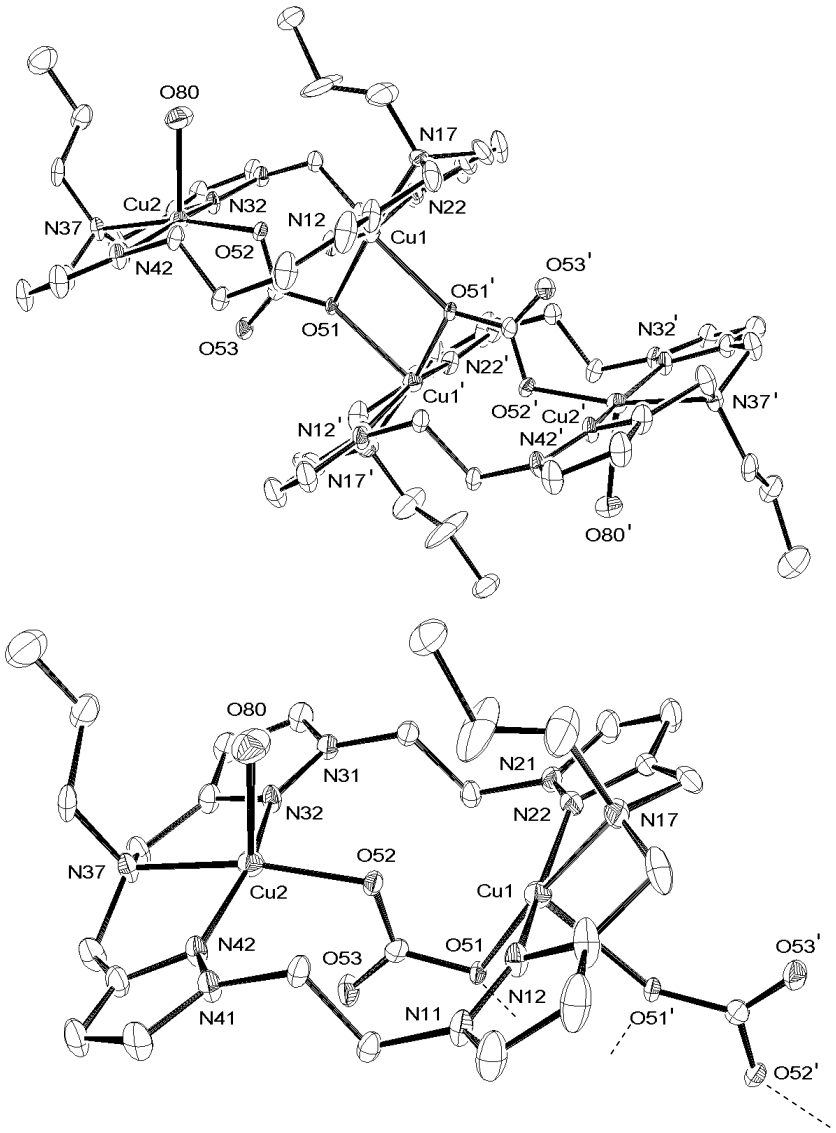

Figure 8.3. ORTEP projection of the tetranuclear cation $[Cu_2([22]pr4pz)(CO_3)(H_2O)]_2^{4+}$ ($(\mathbf{1})_2^{4+}$) (top) and ORTEP projection of half of the tetranuclear cation ($\mathbf{1}^{2+}$) (bottom). Hydrogen atoms and solvent molecules are omitted for clarity. Symmetry operation ': 2-x, y, 0.5-z.

The coordination sphere around the Cu1 ion can be described as a weakly distorted square pyramid ($\tau = 0.23$),[4] with the atoms N12, N17, N22 and O51 occupying the basal plane and the oxygen atom O51' at a distance of 2.330(3) Å occupying the apical position (Figure 8.3, bottom). All copper-nitrogen distances are approximately equal (the average Cu1–N distance is 2.03 Å), whereas the O51 atom is located at a somewhat shorter distance of 1.926(3) Å. The oxygen atom O52 from a bridging

carbonate anion is located at a distance of 2.595(3) Å; however, the very small O52–Cu1–O51a angle of 135.17(11)° suggests that the Cu1 coordination sphere should be considered as a square pyramidal rather than octahedral. Similarly, the coordination geometry around the Cu2 ion can also be best described as a weakly distorted square pyramid ($\tau = 0.1$),[4] in which the basal plane is occupied by the nitrogen atoms N32, N37 and N42 at an average distance of 2.02 Å, and the oxygen atom O52 at the distance of 1.957(3) Å. The axial position is occupied by the oxygen O80 atom from a coordinated water molecule at a distance of 2.267 (4) Å. The oxygen atom O53 is also located in a close proximity of the Cu2 ion (the Cu2-O53 distance is 2.709(4) Å) and could be considered as (semi-)coordinated; however, the very small O80–Cu2–O53 angle of 142.09(14)° does not permit the Cu2 coordination sphere being described as an octahedron.

The crystal packing was found to be uneventful, with only van der Waals interactions realized in the crystal lattice.

Table 8.2. Selected bond lengths and angles for $[Cu_2([22]pr4pz)(CO_3)(H_2O)]_2(CF_3SO_3)_4 \cdot 2CH_3CN \cdot 4H_2O$

Bond lengths (Å)			
Cu1…Cu1'	3.281(2)	Cu1…Cu2	4.5427(18)
Cu1 – O51	1.926(3)	Cu2 – O52	1.957(3)
Cu1 – O51'	2.330(3)	Cu2 – O80	2.267(4)
Cu1 – N12	2.030(5)	Cu2 – N32	1.989(5)
Cu1 – N17	2.025(4)	Cu2 – N37	2.087(4)
Cu1 – N22	2.028(5)	Cu2 – N42	1.998(5)

Bond angles (°)			
O51 – Cu1 – N12	99.94(15)	O52 – Cu2 – O80	87.38(15)
O51 – Cu1 – N17	174.55(16)	O52 – Cu2 – N32	97.65(14)
O51 – Cu1 – N22	99.54(15)	O52 – Cu2 – N37	166.99(15)
O51 – Cu1 – O51'	79.47(13)	O52 – Cu2 – N42	96.75(14)
N12 – Cu1 – N17	80.9(2)	O80 – Cu2 – N32	96.99(16)
N12 – Cu1 – N22	160.18(16)	O80 – Cu2 – N37	105.60(16)
N12 – Cu1 – O51'	92.46(14)	O80 – Cu2 – N42	96.00(16)
N17 – Cu1 – N22	80.0(2)	N32 – Cu2 – N37	81.92(17)
N17 – Cu1 – O51'	95.13(14)	N32 – Cu2 – N42	160.99(16)
N22 – Cu1 – O51'	94.69(14)	N37 – Cu2 – N42	81.25(17)

Symmetry operation: ' = 2-x, y, 1/2-z

$[Cu_2([22]pr4pz)(CH_3CN)_2](ClO_4)_2$

An ORTEP projection of the complex cation $\mathbf{2}^{2+}$ is shown in Figure 8.4. Selected bond lengths and angles are presented in Table 8.3.

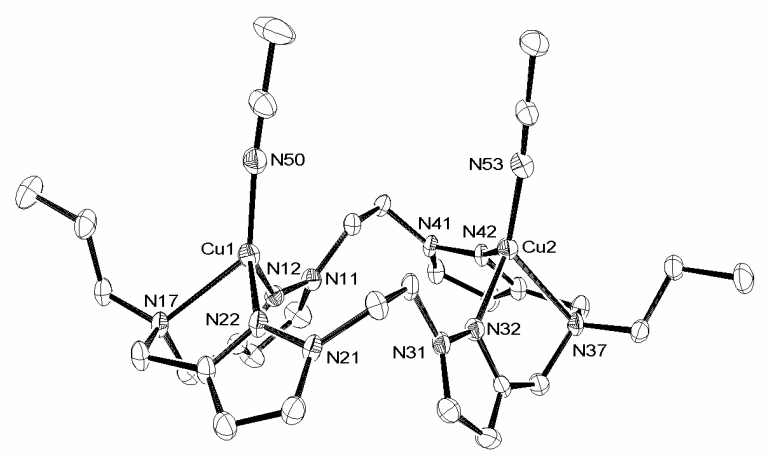

Figure 8.4. ORTEP projection of the complex cation $[Cu_2([22]pr4pz)(CH_3CN)_2]^{2+}$ ($\mathbf{2}^{2+}$). Hydrogen atoms are omitted for clarity.

Table 8.3. Selected bond lengths and bond angles for $[Cu_2([22]pr4pz)(CH_3CN)_2](ClO_4)_2$ ($\mathbf{2}(ClO_4)_2$).

Bond distances (Å)			
Cu1…Cu2	5.547(2)		
Cu1 – N12	2.028(2)	Cu2 – N32	2.055(2)
Cu1 – N17	2.292(2)	Cu2 – N37	2.277(2)
Cu1 – N22	2.063(2)	Cu2 – N42	2.085(2)
Cu1 – N50	1.897(2)	Cu2 – N53	1.903(2)

Bond angles (°)			
N12 – Cu1 – N17	79.47(8)	N32 – Cu2 – N37	79.64(7)
N12 – Cu1 – N22	112.09(8)	N32 – Cu2 – N42	110.05(8)
N12 – Cu1 – N50	121.36(9)	N32 – Cu2 – N53	123.26(9)
N17 – Cu1 – N22	78.20(8)	N37 – Cu2 – N42	78.06(8)
N17 – Cu1 – N50	131.82(8)	N37 – Cu2 – N53	132.19(8)
N22 – Cu1 – N50	121.24(9)	N42 – Cu2 – N53	120.69(9)

Similarly to the structure of the earlier reported dicopper(I) complex with the related macrocyclic ligand [22]py4pz, the macrocyclic ligand adopts a saddle-shaped conformation.[1] However, in [22]py4pz complex the tertiary nitrogen atoms of the ligand fail to bind to the metal ions, resulting in distorted trigonal surroundings for both copper(I) ions. In $\mathbf{2}(ClO_4)_2$, on the contrary, both copper ions are tetracoordinated and have a distorted tetrahedral surrounding, with three positions in the coordination sphere being occupied by the nitrogen donor atoms from the ligand (N12, N17, N22 and N32,

N37, N42) and one by the nitrogen atom of an acetonitrile molecule (N50 and N53). The tripodal nitrogen donor atoms N17 and N37 are located at somewhat longer distances (2.292(2) Å and 2.277(2) Å, respectively) than the nitrogen atoms of the pyrazolyl rings of the ligand (the average Cu1-$N_{pyrazole}$ distance is 2.05 Å, the average Cu2-$N_{pyrazole}$ distance is 2.07 Å). The nitrogen atoms N50 and N53 of the acetonitrile molecules are located, on the contrary, at shorter distances of 1.897(2) Å and 1.903(2) Å, respectively. The N–Cu–N angles for both copper(I) ions vary in quite a large range, *viz.* from 78 to 132°, indicating a significant distortion of the coordination sphere from a regular tetrahedral geometry. The distance between the two copper(I) ions is very large, *viz.* 5.547(2) Å.

8.2.3 Solution stability of $(\mathbf{1})_2(CF_3SO_3)_4{\cdot}2CH_3CN{\cdot}4H_2O$

ESI-MS spectra of $(\mathbf{1})_2(CF_3SO_3)_4{\cdot}2CH_3CN{\cdot}4H_2O$, recorded in a methanol solution (0.2 mM), are characterized by two peaks at *m/z* = 827 and *m/z* = 1801, which correspond to the monocharged dinuclear $\{[Cu_2([22]pr4pz)(CO_3)](CF_3SO_3)\}^+$ and the tetranuclear $\{[Cu_2([22]pr4pz)(CO_3)]_2(CF_3SO_3)_3\}^+$ cation moieties, respectively, and are in agreement with the theoretical isotopic patterns. The tetranuclear copper(II) core stability in methanol solution and its dependence on the concentration was studied by EPR spectroscopy. The EPR spectrum of the solid sample of $(\mathbf{1})_2(CF_3SO_3)_4{\cdot}2CH_3CN{\cdot}4H_2O$ recorded at 13 K is dominated by a strong isotropic signal (g = 2.14), which is characteristic for copper(II) ions experiencing short-range metal-metal exchange interactions, leading to exchange narrowing. The spectrum of $(\mathbf{1})_2(CF_3SO_3)_4{\cdot}2CH_3CN{\cdot}4H_2O$, recorded in KBr matrix (1%), exhibits identical features (Figure 8.5, left, dotted line). The spectrum of a 14 mM solution of the complex in methanol (for simplicity, the complex concentration is calculated based on the molecular weight of the dinuclear species $[Cu_2([22]pr4pz)(CO_3)(H_2O)](CF_3SO_3)_2{\cdot}CH_3CN{\cdot}2H_2O$) also contains a strong isotropic signal with the same g-value; however, the typical features of a triplet spectrum, characteristic for the dinuclear copper(II) species, are also observed (Figure 8.5, left). Upon further dilution, the relative intensity of the isotropic signal gradually diminishes, until at a 0.5 mM concentration a typical triplet spectrum is finally observed. The isotropic signal, observed in the solid state, is likely to be caused by the copper-copper interactions within the tetranuclear core, which are also dominating in a concentrated (14 mM) solution. However, upon dilution, the dissociation of the tetranuclear cluster into two dinuclear species $\mathbf{1}^{2+}$ leads to a typical triplet dicopper(II) spectrum, which gradually increases in relative intensity on the expense of the original isotropic signal.

EPR studies have also been performed in a frozen solution of acetonitrile. The spectrum practically does not change upon dilution, with the strong isotropic signal remaining dominant in the spectrum (0.4–2 mM, Figure 8.5, right), suggesting that the tetranuclear core remains largely intact in this solvent.

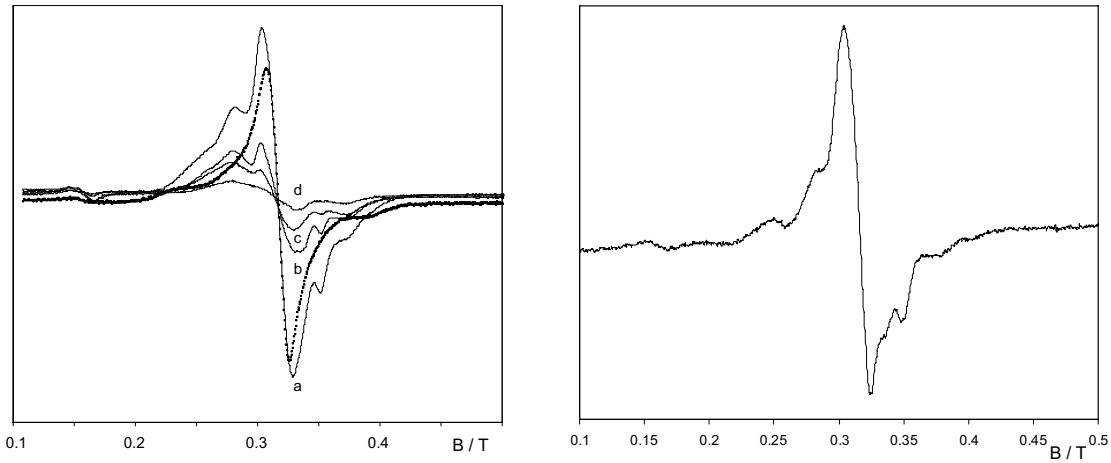

Figure 8.5. Left: Dotted line: EPR spectrum of $(\mathbf{1})_2(CF_3SO_3)_4{\cdot}2CH_3CN{\cdot}4H_2O$ in the solid state (1% in KBr matrix); solid lines: changes in the EPR spectrum of $(\mathbf{1})_2(CF_3SO_3)_4{\cdot}2CH_3CN{\cdot}4H_2O$ in methanol solution upon dilution (a: 14 mM, b: 2 mM, c: 1 mM, d: 0.5 mM) at 13.3 K. Right: EPR spectrum of $(\mathbf{1})_2(CF_3SO_3)_4{\cdot}2CH_3CN{\cdot}4H_2O$ in acetonitrile (2 mM) at 13 K.

8.2.4 Electrochemical properties of $(\mathbf{1})_2(CF_3SO_3)_4{\cdot}2CH_3CN{\cdot}4H_2O$ and $\mathbf{2}(ClO_4)_2$

The electrochemical properties of the complexes were studied by cyclic voltammetry (CV) in methanol and in acetonitrile, using tetrabutylammonium triflate as a supporting electrolyte in case of $\mathbf{1}^{2+}$ ($N\textit{n}Bu_4ClO_4$ could not be used, as the complex precipitates as a perchlorate salt) and tetrabutylammonium perchlorate in case of $\mathbf{2}^{2+}$. The potentials were referred to Ag/10 mM $AgNO_3$ in acetonitrile. In the negative range of potentials, the CV curve of $\mathbf{1}^{2+}$ in MeOH (0.63 mM) is characterized by one irreversible electrochemical signal at E_{pc} = -0.62 V (Figure 8.6, left). Coulometric titrations indicate that this peak corresponds to a one-electron transfer per copper center, resulting in the formation of Cu^{I} species, its re-oxidation being seen on the reverse scan as an irreversible peak at E_{pa} = 0.14 V. Apparently, the mixed-valenced $Cu^{II}Cu^{I}$ species is not formed and cannot be isolated, the copper centers in $\mathbf{1}^{2+}$ being electrochemically equivalent. This result was further confirmed following the changes in the EPR spectrum upon electrochemical reduction of the complex $\mathbf{1}^{2+}$. Since the typical triplet dicopper(II) spectrum was still observed after one electron transfer per dinuclear entity (Figure 8.7), - only its intensity is decreased by a factor 2, - it is concluded that no mixed-valenced species could be formed. The CV curve of $(\mathbf{1})_2(CF_3SO_3)_4{\cdot}2CH_3CN{\cdot}4H_2O$ in acetonitrile looks rather similar to that in methanol, with E_{pc} = -0.72 V and E_{pa} = 0.18 V. As the tetranuclear core is largely preserved in the latter solvent, whereas in methanol, the complex is mainly present in its dissociated form at the concentration level (0.63 mM) used for electrochemical studies, it can be concluded that the dissociation of the dimacrocyclic unit into two dinuclear fragments does not significantly influence the metal reduction potentials.

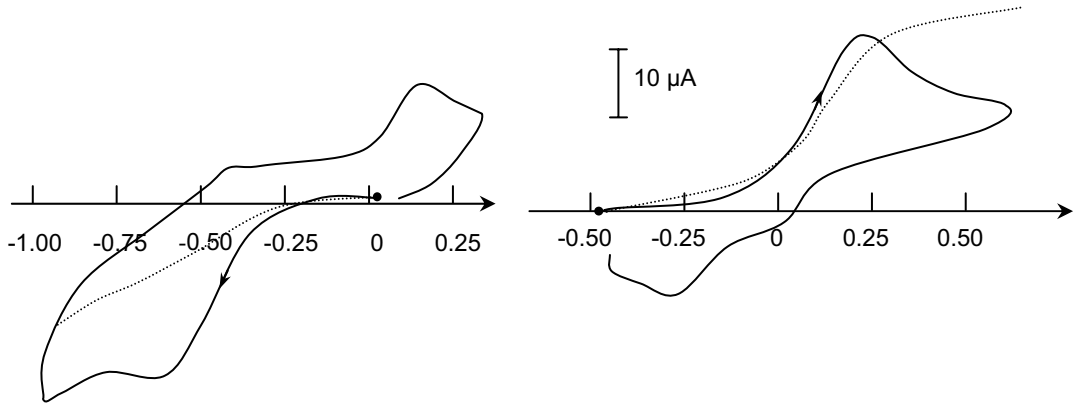

Figure 8.6. Left: electrochemical curves of $\mathbf{1}^{2+}$, recorded in MeOH + 0.1 M N*n*Bu$_4$CF$_3$SO$_3$ on a C disc (∅ = 3 mm); solid line: CV curve, 0.63 mM solution, 0.1 V·s^{-1}, 2 µÅ·cm^{-1}; dotted line: RDE curve, 0.35 mM, 0.01 V·s^{-1}, 5 µÅ·cm^{-1}, N = 600 rpm. Right: Electrochemical curves of $\mathbf{2}^{2+}$, recorded in MeOH + 0.1 M N*n*Bu$_4$ClO$_4$ on a C disc (∅ = 3 mm); solid line: CV curve, 1 mM solution, 0.1 V·s^{-1}; dotted line: RDE curve, 0.65 mM, 0.01 V·s^{-1}, N = 600 rpm.

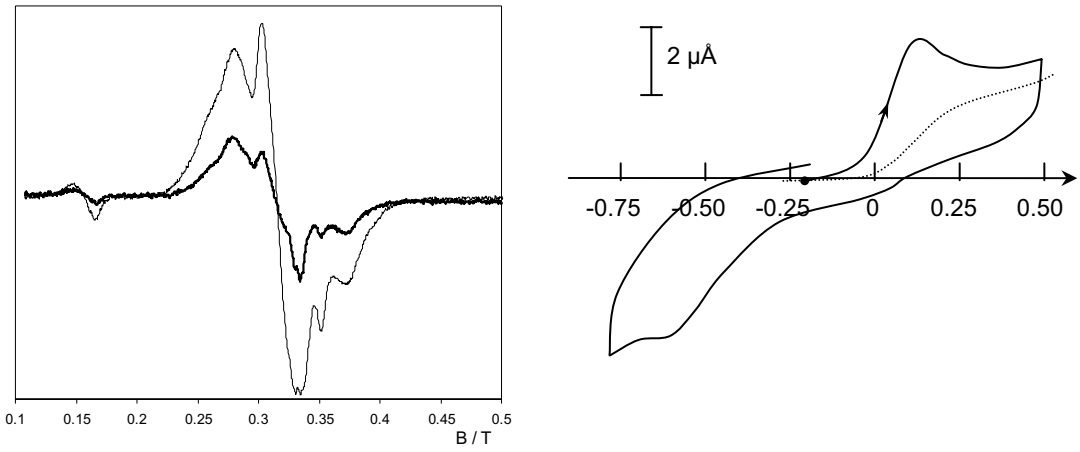

Figure 8.7. Left: Changes in the EPR spectrum at 13 K of $\mathbf{1}^{2+}$ (1 mM solution in MeOH) upon electrolysis. The solid line corresponds to the original spectrum, the bold line corresponds to the spectrum recorded after one-electron reduction. Right: Electrochemical curves of $\mathbf{1}^{2+}$ (1 mM, MeOH + 0.1 M N*n*Bu$_4$CF$_3$SO$_3$, a C disc (∅ = 3 mm)) after one-electron reduction; solid line: CV curve, 0.1 V·s^{-1}, dotted line: RDE curve, 0.01 V·s^{-1}, N = 600 rpm.

The CV curve of $\mathbf{2}^{2+}$ in methanol is characterized by one broad electrochemical signal at E_{pa} = 0.22 V, *i.e.* at a potential close to the one (0.14 V) observed for the Cu^{I} species electrogenerated from $\mathbf{1}^{2+}$ (Figure 8.6, right). This small difference accounts likely for small discrepancy in the coordination spheres around the copper(I) center between the two complexes, *e.g.* caused by the initial presence of coordinated water molecules in $\mathbf{1}^{2+}$ and acetonitrile molecule in $\mathbf{2}^{2+}$ or the carbonate bridge in the copper

coordination sphere in $\mathbf{1}^{2+}$ (the carbonate bridge, however, is expected to dissociate upon electrochemical reduction due to its poor ability to bridge two copper(I) centers). Coulometric titration shows that this anodic process corresponds to a one electron transfer per copper center leading to Cu^{II} species. The reduction of the electrogenerated two-electron oxidized species from $\mathbf{2}^{2+}$ is seen on the CV curve, during the reverse scan, as two ill-resolved peaks at E_{pc1} = 0.03 V and E_{pc2} = -0.45 V, suggesting the presence of two different electrogenerated Cu^{II} species, likely accounting for different re-coordinations with solvent molecules.

8.2.5 Magnetic properties of $(\mathbf{1})_2(CF_3SO_3)_4{\cdot}2CH_3CN{\cdot}4H_2O$

The thermal dependence of the complex χT (where χ is the magnetic susceptibility per Cu_2 formula unit) is plotted in Figure 8.8. χT gradually increases upon lowering the temperature from 0.84 $cm^3{\cdot}mol^{-1}{\cdot}K$ at 300 K to reach a maximum around 0.95 $cm^3{\cdot}mol^{-1}{\cdot}K$ at 15 K. A decrease is then observed down to 0.81 $cm^3{\cdot}mol^{-1}{\cdot}K$ at 5 K. Values at high temperatures are in agreement with two uncoupled spin 1/2 centers (*e.g.* 0.75 $cm^3{\cdot}mol^{-1}{\cdot}K$ for g = 2), while the increase observed is the signature of intramolecular ferromagnetic interactions. The full Hamiltonian describing the pairwise interactions among the Cu^{II} ions in $(\mathbf{1})_2(CF_3SO_3)_4{\cdot}2CH_3CN{\cdot}4H_2O$, can be expressed by equation 8.1:

$$H = -2J_1(S_1 \cdot S_2 + S_{1'} \cdot S_{2'}) - 2J_2(S_1 \cdot S_{1'}) - 2J_3(S_1 \cdot S_{2'} + S_{1'} \cdot S_2) - 2J_4(S_2 \cdot S_{2'}) \quad (8.1)$$

where the structural numbering scheme has been kept. The energy levels and their spin quantum numbers were derived previously.[5] Testing the influence of each interaction parameter on the quality of the fit, J_4 was found to be of no influence, while J_3 was found to be undetermined when allowed to vary freely together with J_2. Indeed, although it was observed in a specific case,[5] a significant coupling between fourth neighbouring spins (J_4) is unlikely. On the other hand, given the low spin density in the axial position for a close to square-pyramidal coordination environment, the central coupling pathway through the two oxygen atoms respectively in axial and equatorial positions (J_2) can be expected to be more significant than that through the carbonato bridge with again one axial and one equatorial oxygen atom (J_3). Thus, and in light of these magneto-structural considerations, J_3 and J_4 were fixed to 0. Then the best fit parameters were J_1/k_B = 11.4(5) K, J_2/k_B = –3.49(4) K and g = 2.10(1), with a Temperature Independent Paramagnetism term at TIP = $6.6(3)\times10^{-4}$ $cm^3{\cdot}mol^{-1}$. It should be noted that a small negative value of J_3 (< 1 K) is likely, but could not be determined with accuracy, given its interdependence with J_2, and its small influence on the quality of the fit. The resulting low-lying states are then a singlet ground state with a triplet state and a quintuplet state at respectively *ca.* 1.4 K and 5.4 K above it. The ferromagnetic coupling propagated through the *syn*, *syn* carbonato bridge is in agreement with previous observations in dinuclear[6] and trinuclear[7,8] compounds with a

syn-syn bridging coordination mode. On the other hand, because of the low spin density in axial d_{z^2} orbital, only a weak antiferromagnetic interaction, such as that found for J_2, can be expected from the orbital overlap through the asymmetric di-μ-$O_{carbonate}$ bridge.

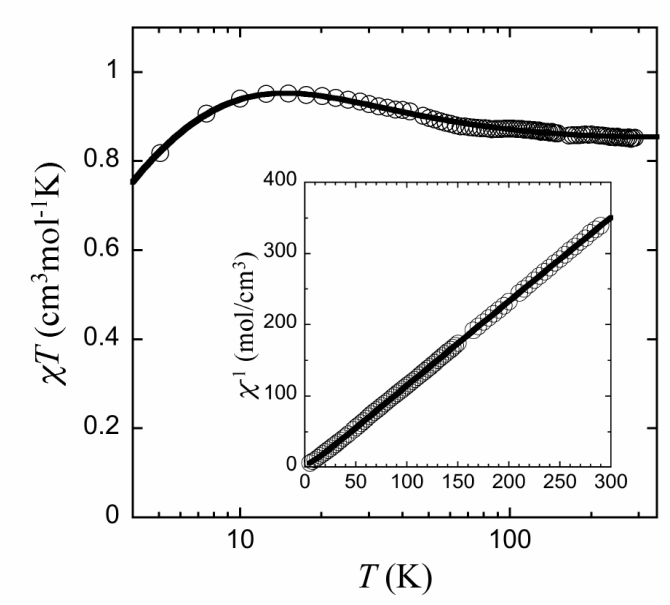

Figure 8.8. Semi-logarithmic plot of χT *vs.* T for $(\mathbf{1})_2(CF_3SO_3)_4{\cdot}2CH_3CN{\cdot}4H_2O$ under a 0.1 T applied field, where χ is the magnetic susceptibility per Cu_2 formula unit. The inset shows the thermal dependence of the inverse magnetic susceptibility. Full lines represent the best fit obtained with a tetranuclear model (see text for further details).

8.2.6 Catecholase activity of $(\mathbf{1})_2(CF_3SO_3)_4{\cdot}2CH_3CN{\cdot}4H_2O$

8.2.6.1 Kinetic studies

The catalytic oxidation of the model substrate $DTBCH_2$ (3,5-di-*tert*-butylcatechol) by $(\mathbf{1})_2(CF_3SO_3)_4{\cdot}2CH_3CN{\cdot}4H_2O$ was evaluated spectrophotometrically in dioxygen-saturated methanol by monitoring the increase in absorbance at 400 nm, corresponding to the formation of the quinone product DTBQ (3,5-di-*tert*-butyl-*o*-benzoquinone). The initial reaction rates were determined from the slope of the trace at 400 nm during the first 0.7 minutes of the reaction, when the absorption at 400 nm increases linearly. Because the concentration of the complex, used for the catecholase activity studies, was 2×10^{-5} M, the active species can be regarded as dinuclear.

The $DTBCH_2$ oxidation rate was found to be strongly dependent on the substrate concentration. The rate-determining step was found to change with the substrate to complex ratio. Thus, at low substrate to complex ratios (< 12:1, $[\mathbf{1}^{2+}] = 2\times10^{-5}$ M), the reaction shows Michaelis-Menten behavior (Figure 8.9, right). The Lineweaver-Burk treatment gives $K_M = 0.176$ mM and $V_{max} = 2.47\times10^{-6}$ M·s^{-1}. This behavior indicates the presence of equilibrium in the rate-determining step. At high substrate to complex ratios

(up to 200:1), the reaction rate depends linearly on the $DTBCH_2$ concentration, with the 1st order rate constant $k_1 = 2\times10^{-4}$ s^{-1} ($R^2 = 0.9986$, Figure 8.9, left).

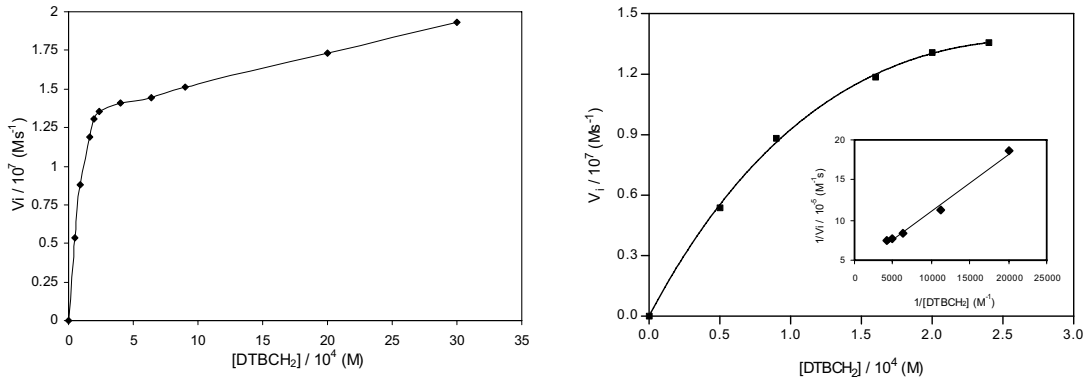

Figure 8.9. Left: the dependence of the initial reaction rates on catechol concentration, as determined from the slope of trace at 400 nm in the first 0.7 min of the catalytic reaction. Right: the dependence of the initial reaction rates on catechol concentration for substrate to catalyst ratios below 12:1 ([$\mathbf{1}^{2+}$] = 2×10^{-5} M), the insert shows the reciprocal Lineweaver-Burk plot ($R^2 = 0.9932$).

A linear dependence on the complex concentration in the whole concentration range at all substrate to complex ratios was found (Figure 8.10).

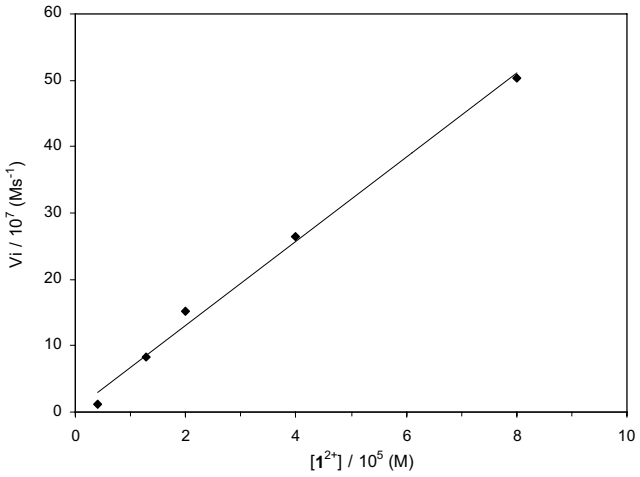

Figure 8.10. Dependence of the initial reaction rates on the concentration of $\mathbf{1}^{2+}$ in the catalytic oxidation of $DTBCH_2$ in methanol solution ([$DTBCH_2$] = 1 mM, $k_2 = 0.063$ s^{-1}, $R^2 = 0.9945$).

The catalytic reaction is finished within a few minutes at low catechol to complex ratios, whereas at high catechol to complex ratios, no full conversion of $DTBCH_2$ could be achieved, not even after 24 hours. To evaluate whether the reaction rate may be influenced by the formed product DTBQ, the kinetic studies in the presence of variable amounts of added quinone were performed. DTBQ was indeed found to have a strong inhibiting effect on the catalytic process, as can be seen from Figure 8.11. For instance, the initial reaction rate was found to decrease to 50% of its initial value in the presence of *ca.* 5 molar equivalents of DTBQ. This inhibiting effect was observed both at low (10:1) and high (50:1) catechol to complex ratios ([$\mathbf{1}^{2+}$] = 2×10^{-5} M).

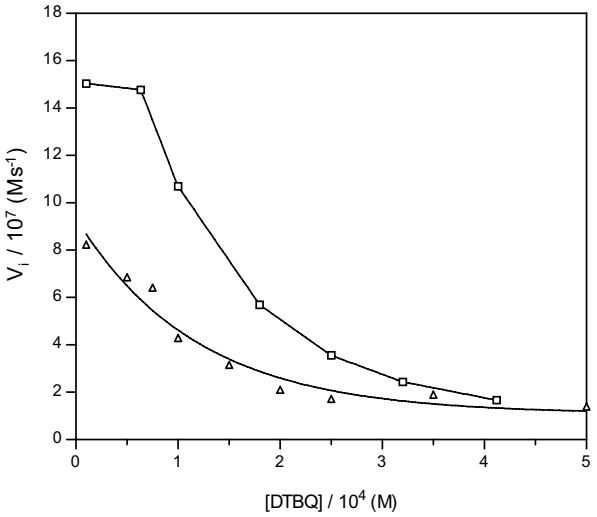

Figure 8.11. Dependence of the initial reaction rates on the concentration of DTBQ at low (∆, 10:1) and high (□, 50:1) $DTBCH_2$ to complex ratios ([$\mathbf{1}^{2+}$] = 2×10^{-5} M).

Interestingly, $(\mathbf{1})_2^{4+}$ does not exhibit catecholase activity in acetonitrile. Instead, only one equivalent of quinone is formed stoichiometrically. The plot of the initial reaction rates *vs.* catechol concentration indicates a substrate saturation behavior (Figure 8.12, left). The reciprocal Lineweaver-Burk plot (Figure 8.12, right) gives K_M = 0.42 mM and $V_{max} = 5\times10^{-7}$ $M^{-1}\cdot s^{-1}$.

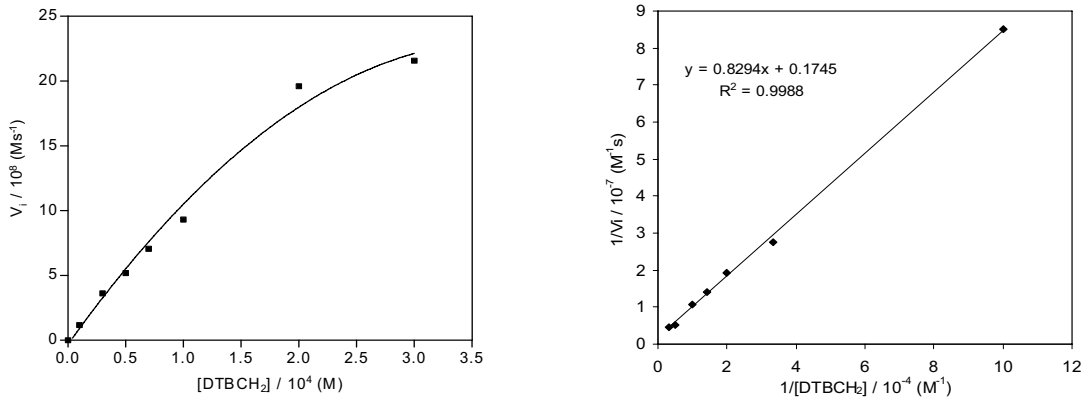

Figure 8.12. The dependence of the initial reaction rates on catechol concentration for the stoichiometric quinone formation in CH_3CN (left) and the reciprocal Lineweaver-Burk plot (right). [complex] = 2×10^{-5} M (the concentration calculated based on the molecular weight of the dinuclear species $[Cu_2([22]pr4pz)(CO_3)(H_2O)]\cdot CH_3CN\cdot 2H_2O$).

8.2.6.2 Formation of H_2O_2 and its influence on the reaction

The reduction of dioxygen to dihydrogen peroxide upon catechol oxidation by copper(II) complexes has been previously established only in a few cases.[9-12] The formation of H_2O_2 in the course of the catalytic reaction has been studied for two different catechol to complex ratios (10:1 and 50:1, [$\mathbf{1}^{2+}$] = 2×10^{-5} M). In both cases,

dihydrogen peroxide was formed at the initial stage of the reaction, and its formation was found to practically stop after a few minutes, although the oxidation of $DTBCH_2$ was still continuing (Figure 8.13). This suggests that two different mechanisms may be operating during the catalytic oxidation of $DTBCH_2$ by $\mathbf{1}^{2+}$: one, in which dioxygen undergoes a two-electron reduction to dihydrogen peroxide, and a second mechanism, in which it is converted into water upon four-electron reduction.

In order to evaluate the influence of dihydrogen peroxide on the catalytic reaction, catalytic studies were performed in the presence of variable amounts of H_2O_2. The plot of the initial reaction rates *vs.* dihydrogen peroxide concentrations is depicted in Figure 8.14. As can be seen, at low H_2O_2 concentrations its presence has virtually no influence on the reaction rates. At higher concentrations (above 20 molar equivalents of H_2O_2 per one mole of the complex), it accelerates the reaction rate. However, the concentration of dihydrogen peroxide, formed during the reaction, does not reach this level (Figure 8.13).

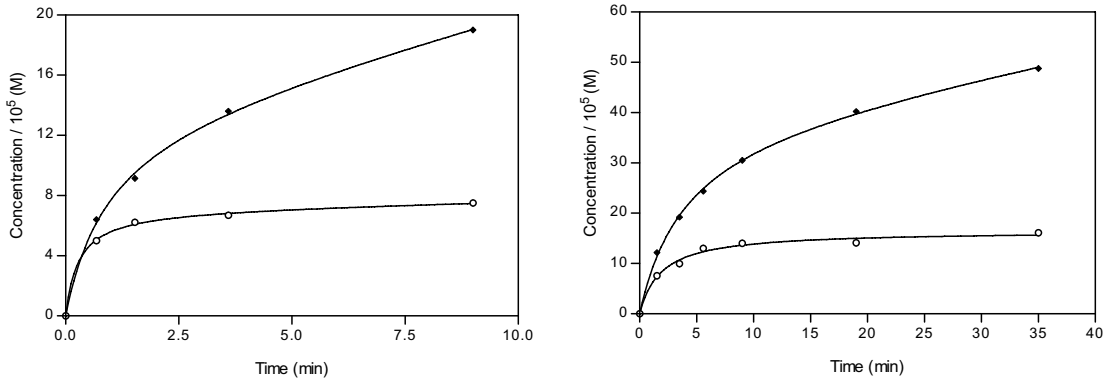

Figure 8.13. The course of DTBQ (◆) and H_2O_2 (○) formation during the catalytic reaction at low (10:1, left) and high (50:1, right) substrate to catalyst ratios ([$\mathbf{1}^{2+}$] = 2×10^{-5} M).

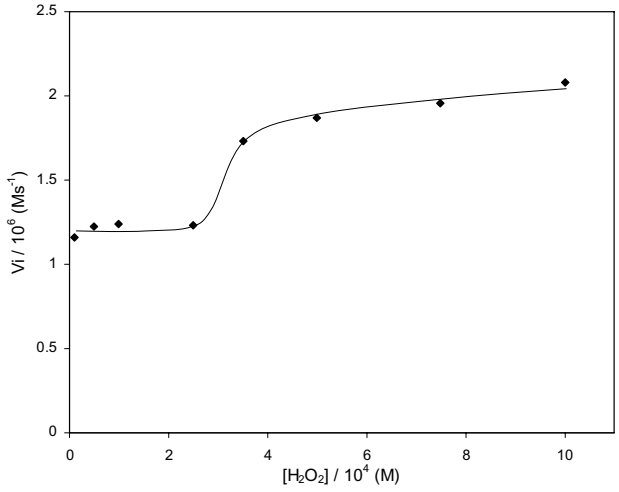

Figure 8.14. Dependence of the initial reaction rates in the catalytic oxidation of $DTBCH_2$ by $\mathbf{1}^{2+}$ in MeOH on the dihydrogen peroxide concentration. The initial concentration of $DTBCH_2$ is 1 mM, the concentration of $\mathbf{1}^{2+}$ is 2×10^{-5} M.

8.2.6.3 Anaerobic interaction of 1^{2+} and 2^{2+} with $DTBCH_2$ and DTBQ

As shown previously by Krebs and co-authors,[13] the catalytic cycle of catechol oxidase starts with the native *met* state of the enzyme, which reacts stoichiometrically with catechol, producing one equivalent of the quinone and leading to the dicopper(I) (*deoxy*) form. The anaerobic interaction of $\mathbf{1}^{2+}$ with $DTBCH_2$ has been studied spectrophotometrically. Upon addition of one molar equivalent of $DTBCH_2$ to a 0.5 mM solution of $\mathbf{1}^{2+}$ in methanol, two new absorptions at 389 nm (ε = 2920 $M^{-1}\cdot cm^{-1}$) and 760 nm (ε = 359 $M^{-1}\cdot cm^{-1}$) gradually develop in the spectrum (Figure 8.15, left). Both bands are characteristic of the formation of the semiquinone radical[14] and suggest that $\mathbf{1}^{2+}$ reacts with $DTBCH_2$, while undergoing a one-electron reduction, leading to the formation of mixed-valenced $Cu^{II}Cu^{I}$-semiquinone species (DTSQ). The rate constant k_3 of this process is 1.8×10^{-3} $M^{-1}\cdot s^{-1}$. The addition of an excess of $DTBCH_2$ (up to five molar equivalents) has no influence on the spectrum. The formed semiquinone species is stable for at least 24 hours under anaerobic conditions.

These results were further confirmed by EPR spectroscopy (Figure 8.15, right). The EPR spectrum of a 1 mM frozen solution in MeOH of $\mathbf{1}^{2+}$ in the presence of one molar equivalent of $DTBCH_2$ is characterized by a typical axial signal of mononuclear Cu^{II} species ($g_{//}$ = 2.23, $A_{//} = 175\times10^{-4}$ cm^{-1}, $g\perp$ = 2.04) and a sharp signal centered at g = 2.00 corresponding to an organic radical. The results explicitly show the absence of interaction between the two metal centers, indicating the presence of discrete Cu^{II} and Cu^{I} ions within the complex, and the absence of interaction between the semiquinone radical and the Cu^{II} ion.

The electrochemical behavior of the mixed-valenced $Cu^{II}Cu^{I}$-semiquinone species has been also examined. The CV curve, recorded in a 0.5 mM methanolic solution of $\mathbf{1}^{2+}$ in the presence of one molar equivalent of $DTBCH_2$, is characterized in the negative region of potentials by a quasi-reversible electrochemical signal at $E_{1/2}$ = -0.34 V (Figure 8.16), which is followed at lower potential by the copper(0) deposition onto the electrode surface. Based on earlier reported electrochemical properties of the semiquinone species,[15,16] this signal has been assigned to the one-electron reduction of the semiquinone radical. However, a close examination of this signal shows that it displays a shoulder suggesting the presence of two overlapping electrochemical systems. It is likely that the reduction process of the Cu^{II} center in the mixed-valenced $Cu^{II}Cu^{I}$-semiquinone species is hidden underneath the electrochemical response of the semiquinone moiety. In the positive range of potentials, the electrochemical curve is characterized by two ill-resolved oxidation waves at E_{pa} = 0.12 V and E_{pa} = 0.42 V (Figure 8.16), associated with the electrochemical responses of the $Cu^{II}Cu^{I}$ / $Cu^{II}Cu^{II}$ redox couple and the one-electron oxidation of the semiquinone radical.

It is interesting to note that mixed-valenced $Cu^{II}Cu^{I}$ species forms readily upon anaerobic reaction of $\mathbf{1}^{2+}$ with $DTBCH_2$, whereas they could not be generated

electrochemically. These results suggest an asymmetric binding of the substrate to only one of the two copper centers of the dinuclear subunit $\mathbf{1}^{2+}$ prior to the redox reaction, leading to the differentiation of the two metal centers. This in turn results in their different reduction potentials, allowing the subsequent formation of the mixed-valenced dicopper core.

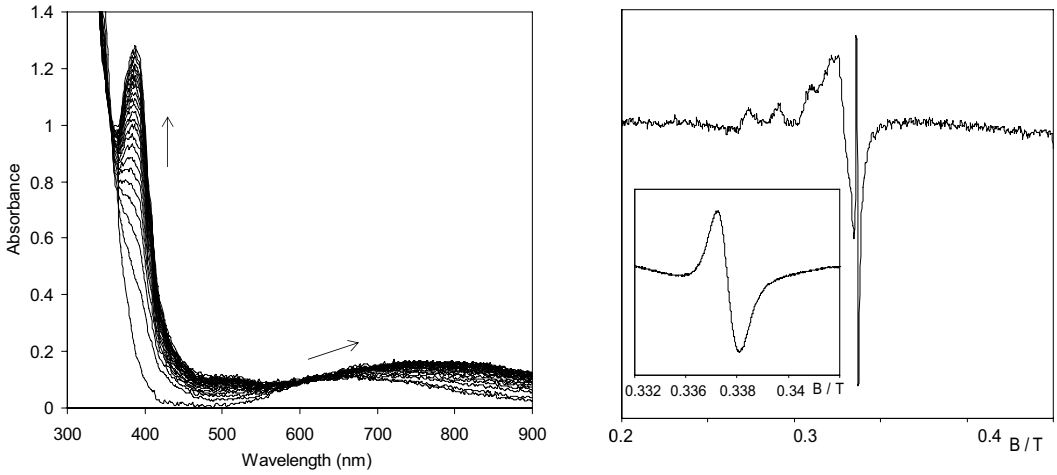

Figure 8.15. Left: changes in the UV-Vis spectrum upon addition of 1 eq. $DTBCH_2$ to a methanolic solution of $\mathbf{1}^{2+}$ (0.5 mM) in anaerobic conditions at 100 K. Right: the EPR-spectrum of the resulting mixed-valenced $Cu^{II}Cu^{I}$-semiquinonate species in anaerobic conditions (1 mM solution of $\mathbf{1}^{2+}$ in methanol, 100 K). Insert: the enlarged signal of the semiquinone radical.

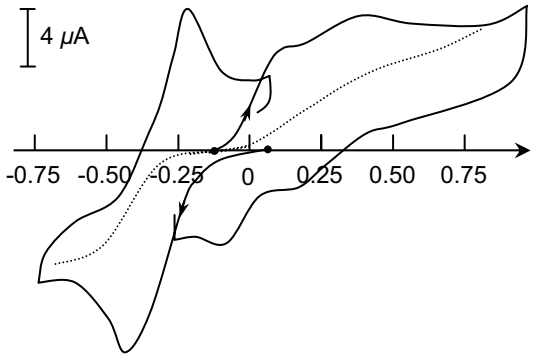

Figure 8.16. Electrochemical curves of $\mathbf{1}^{2+}$ (0.5 mM) in the presence of one equivalent of $DTBCH_2$, recorded in MeOH + 0.1 M $N\mathit{n}Bu_4CF_3SO_3$ on a C disc (∅ = 3 mm). Solid line: CV curves, 0.1 $V{\cdot}s^{-1}$; dotted line: RDE curves, 0.01 $V{\cdot}s^{-1}$, N = 600 rpm.

The mixed-valence $Cu^{II}Cu^{I}$-semiquinone species was also found to form upon treating the solution of the dicopper(I) complex $\mathbf{2}^{2+}$ (0.5 mM) with one molar equivalent of DTBQ under anaerobic conditions. In contrast to the slow reaction of $\mathbf{1}^{2+}$ with $DTBCH_2$, upon reaction of $\mathbf{2}^{2+}$ with the quinone the redox process occurs immediately, precluding the determination of the reaction rate constant. Upon exposing the resulting solution to dioxygen, the characteristic bands of semiquinone at 389 nm and 760 nm

gradually diminish, with an isosbestic point at 460 nm, indicating its oxidation by dioxygen. Accordingly, the radical signal in the EPR spectrum disappears, and an increase of the absorption at 400 nm in the UV-Vis spectrum indicates the formation of the quinone. The iodometric H_2O_2 assay test in the presence of lactoperoxidase indicates that this process is accompanied by the formation of one equivalent of dihydrogen peroxide as a side product.

8.2.6.4 Mechanisms *vs.* a coordination mode of the substrate

Based on the results reported above it is possible to suggest the mechanism of catechol oxidation by $\mathbf{1}^{2+}$, as depicted in Figure 8.17. The catalytic cycle starts with the anaerobic oxidation of $DTBCH_2$ by $\mathbf{1}^{2+}$; however, in contrast to the natural enzyme behavior,[13,17] only one electron is transferred in the stoichiometric reaction between the complex and the substrate, leading to the formation of the mixed-valenced $Cu^{II}Cu^{I}$-semiquinone species. This observation is rather interesting, as the formation of a semiquinone radical as an intermediate species in catechol oxidation has been earlier proposed and/or observed in only a few cases.[10,14,18,19] In most cases, such species was formed upon reaction of catechol with mononuclear[19] or dinuclear[10] Cu^{II} complexes generated by self-assembly of two mononuclear units. In the present case, however, $\mathbf{1}^{2+}$ is essentially dinuclear in solution; nevertheless, the second copper(II) ion does not participate in the redox process, playing solely a structural role.

The formed semiquinone radical is further oxidized by dioxygen, as was confirmed by UV-Vis and EPR spectroscopy. According to the earlier mechanistic reports of Kaizer *et al.*[19] and Kodera *et al.*,[10] dioxygen can bind to the Cu^{I} ion forming a Cu^{II}-superoxo species, with the consequent one-electron oxidation of the semiquinone radical leading to the release of quinone and hydrogen peroxide (Figure 8.17, cycle A). However, in the course of the catalytic oxidation of $DTBCH_2$ by $\mathbf{1}^{2+}$ the concentration of H_2O_2 stops increasing after a few minutes, indicating that, most likely, a different mechanism is operating at later stages of the reaction. A proposal about H_2O_2 being consumed in the course of the reaction, as suggested by some authors,[20] does not seem plausible in this case, as the results of kinetic measurements indicate that its presence has virtually no influence on the catalytic cycle, except at unrealistically high concentrations levels, which are never reached during the reaction. Another reason to suggest a different mechanistic pathway operating at later stages of the catalytic oxidation is the inhibiting effect of DTBQ, indicating that the formed quinone does not simply accumulate in the reaction mixture, but obviously also participates in the catalytic process. This effect cannot be explained based on the simple oxidation scheme via the semiquinone formation (cycle A in Figure 8.17).

Consequently, it can be proposed that at later stages of the catalytic reaction, the oxidation of $DTBCH_2$ proceeds by a “classic” mechanism, proposed by Krebs *et al.*[17] and Casella *et al.*,[21,22] involving a stoichiometric reaction between the dicopper(II)

species and the substrate, leading to the reduced dicopper(I) species. The oxidation of the second equivalent of the substrate by a peroxo-dicopper(II) adduct, formed upon dioxygen binding to the dicopper(I) intermediate, results in the formation the second molecule of quinone and water as a by-product (Figure 8.17, cycle B). The inhibiting effect of DTBQ on the catalytic cycle can then be rationalized considering its very fast reaction with the reduced dicopper(I) species (which is the only intermediate species able to react with the quinone), leading to semiquinone formation (Figure 8.17). Thus, at high concentrations, DTBQ competes with dioxygen in the reoxidation of $\mathbf{2}^{2+}$, resulting in the mixed-valenced $Cu^{II}Cu^{I}$ semiquinone species, which is then subsequently oxidized in the less efficient cycle A. Consequently, the concentration of quinone increases more slowly, as only one molecule of DTBQ is produced in cycle A, contrary to cycle B.

On the other hand, when present in high concentration (Figure 8.14), H_2O_2 can compete with dioxygen in the reoxidation of the dicopper(I) complex to the dicopper(II) state, therefore the increase in its concentration results in its progressive involvement as copper(I) oxidant. The increase of the reaction rates in this case can be explained by a change in the rate-determining step of the reaction, as previously proposed by Casella and co-workers.[21]

The change of the catalytic mechanism in the course of the reaction can be explained by proposing that the different mechanistic pathways are directly related to the binding mode of the substrate to the dicopper(II) core. The latter has often been debated in the literature in the past years.[23-27] Up till now, different examples of substrate coordination modes to dicopper(II) complexes have been reported.[23-25] Although the first example of a dicopper(II)-catecholate adduct, crystallized by Karlin,[23] showed the catecholate to be coordinated as a bridging didentate ligand to both dicopper(II) centers, later reports from Casella[24] and Meyer[25] argued for an asymmetric binding of catechol to only one of the two available copper(II) ions in a η^2 fashion, possibly with one of the two oxygen atoms being involved in a weak interaction with either an adjacent copper(II) ion, or in hydrogen bonding. This apparent contradiction can be rationalized by considering that the binding mode of the substrate is to a large extent determined by the distance between the two copper centers and their accessibility. Thus, the short metal-metal distance promotes a binding of the catecholate in a didentate bridging fashion (*e.g.* in the dicopper(II)-catecholate adduct reported by Karlin[23] two metal ions are kept at a distance of 3.248 Å), whereas in case of long metal-metal separation, a binding of the substrate to only one of the two metal centers occurs. Consequently, in the first case, only one electron can be transferred from the substrate to the metal center, resulting in the semiquinone formation, the subsequent oxidation of which proceeds by the mechanism proposed by Kodera[10] (Figure 8.17, cycle A). In the case of a didentate bridging coordination, both copper ions are reduced in the stoichiometric reaction with the substrate, leading to the quinone formation and the reduced dicopper(I) species, and

the catalytic reaction further proceeds via the mechanism suggested by Krebs *et al.*[17] for the natural enzyme (Figure 8.17, cycle B).

The long Cu1…Cu2 separation (4.5427(18) Å) observed for two copper ions in the macrocyclic unit in $\mathbf{1}^{2+}$ prohibits the substrate binding in a bridging didentate fashion, thus favoring the binding of catechol to only one metal center with semiquinone formation. However, it is liable that in the course of the catalytic reaction the original dicopper(II) core undergoes substantial modification, as the carbonate bridge is likely to be cleaved by the incoming catecholate, as proposed in Figure 8.17. Earlier studies on other dicopper complexes with structurally related macrocyclic ligands[2,28] indicate that the macrocyclic cavity has a sufficient flexibility to bring two copper ions on a short distance, required for a didentate bridging coordination mode of catechol. As a result, in the absence of the rigid carbonate bridge the substrate can bind to both copper(II) ions in a bridging fashion, pushing the catalytic reaction towards the cycle B, whereas the relative influence of mechanistic pathway A becomes negligible after a few minutes of the reaction.

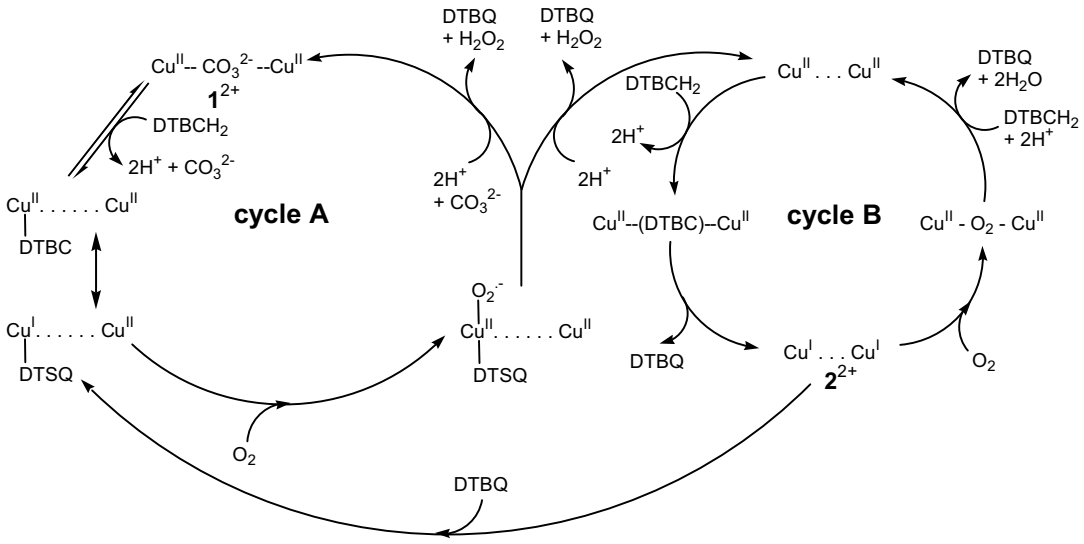

Figure 8.17. The proposed mechanism for the catalytic catechol oxidation by $\mathbf{1}^{2+}$.

8.3 Concluding remarks

It is very interesting to compare the catalytic behavior of $\mathbf{1}^{2+}$ with earlier reported examples of synthetic models of catechol oxidase. The metal-metal distance in the dicopper(II) core of $\mathbf{1}^{2+}$ exceeds 4.5 Å and is thus much longer than the usual range found in catalytically active copper(II) compounds (2.9-3.5 Å). However, $\mathbf{1}^{2+}$ still exhibits catecholase activity, proving that a large copper-copper separation does not inhibit the catalytic properties. Furthermore, the results give an answer to the question, whether the binding of the substrate to the dicopper core includes a bridging catecholate coordinated to the two copper ions[29] rather than a monodentate coordination to only one

metal center,[13] demonstrating that in fact both options are possible. It is also clear that different binding modes of the substrate to a dicopper(II) core result in completely different mechanisms of catechol oxidation by dicopper(II) complexes; furthermore, in case of sufficiently flexible ligands, both mechanistic pathways can be realized.

In addition, a possible mechanism for the formation of dihydrogen peroxide is now established. Previously, it has been suggested that the formation of dihydrogen peroxide is the result of either the protonation of the peroxo-dicopper intermediate, or its reaction with catechol, leading to the formation of the reduced dicopper(I) species along with H_2O_2.[22,25,30] However, no actual proof that either of these pathways indeed takes place has been reported, although the formation of dihydrogen peroxide upon treating trans-μ-1,2-peroxo-dicopper(II) species with a strong acid is well-known.[31,32] Consequently, it can be assumed that dihydrogen peroxide is formed as a by-product during the oxidation of the semiquinone intermediate with dioxygen, when the metal-metal distance within a dicopper(II) complex is too long to allow the binding of the substrate in a didentate bridging fashion. Indeed, Meyer and co-workers reported a recovery of 58% to 71% of dihydrogen peroxide for a series of dicopper(II) complexes,[25] for which an asymmetric coordination mode of a non-reactive catechol to only one of the copper(II) centers has been clearly established. In addition, two other crystallographically characterized dicopper(II) complexes with essentially dinucleating ligands, for which the reduction mode of dioxygen to dihydrogen peroxide has been definitely established, also possess a large metal-metal separation (3.7 Å and 7.8 Å).[12]

It thus appears that the mechanism of catechol oxidation by the model compounds is very intricate, which obviously explains often contradictory literature reports on the catalytic behavior of copper(II) complexes. It is also very interesting to note that some authors have recently reported the formation of dihydrogen peroxide,[33] as well as semiquinone radicals,[34] during the catalytic oxidation of DOPA by the structurally related enzyme tyrosinase in haemolymph of some insects. Although it appears that neither of these species has ever been observed during the substrate oxidation by catechol oxidase, the question about the possibility of two different catechol oxidation pathways for the natural enzyme, as found for model compounds, still needs to be answered.

8.4 Experimental Section

8.4.1 Materials and Methods

All starting materials were commercially available and used as purchased, unless stated otherwise. The macrocyclic ligand [22]pr4pz was synthesized as previously described.[2] The single crystals of $[H_2[22]pr4pz](ClO_4)_2$ suitable for X-ray crystal structure determination were obtained by diethyl ether diffusion into a methanol solution containing one equivalent of [22]pr4pz and two equivalents of perchloric acid.

The ligand field spectra in solution were recorded on a Varian Cary 50 Scan UV-Vis spectrophotometer and on a Zeiss MCS500 Diode-Array Spectrometer (l = 0.5 cm). X-band electron paramagnetic resonance (EPR) measurements were performed on a Bruker ESP 300E spectrometer equipped with a Bruker nitrogen flow cryostat, or on a Bruker EMX spectrometer equipped with an ESR 900 helium flow cryostat (Oxford Instruments). The electrochemical behavior of the complexes was investigated in a 0.1 M solution of tetra-*n*-butylammonium perchlorate (TBAP) or tetra-*n*-butylammonium triflate in methanol using a EGG 273 potentionstat coupled with a Kipp&Zonen x-y recorder. The experiments were performed at room temperature in a three-compartment cell. Potentials are referred to an Ag/10 mM $AgNO_3$ + CH_3CN + 0.1 M TBAP reference electrode. The working electrode was a platinum disk of 5 mm diameter. The working electrode was polished with 1 μm diamond paste prior to each recording. C, H, N, S determinations were performed on a Perkin Elmer 2400 Series II analyzer. ESI-mass spectra in methanol or acetonitrile were recorded on a Bruker Esquire 300 apparatus.

8.4.2 Synthesis of the coordination compounds

$[Cu_2([22]pr4pz)(CO_3)(H_2O)]_2(CF_3SO_3)_4{\cdot}2CH_3CN{\cdot}4H_2O$ ($(1)_2(CF_3SO_3)_4{\cdot}2CH_3CN{\cdot}4H_2O$): Copper(II) triflate (36.9 mg, 0.10 mmol) was dissolved in 5 ml of acetonitrile, and the resulting solution was added to a suspension of the ligand [22]pz4pz (25 mg, 0.05 mmol) in the same solvent (the ligand does not dissolve, unless coordinated to the metal ions). To the resulting clear blue solution, a solution of anhydrous Na_2CO_3 (5.4 mg, 0.05 mmol) in a minimal amount of water was added. The small amount of precipitate, most likely basic copper carbonate, which may form, was filtered off. Diethyl ether diffusion into the resulting greenish-blue solution led to the appearance of small blue crystals which were found to be of a sufficient quality for X-ray single crystal structure determination. Elemental analysis, found (calc.) for $[Cu_2([22]pr4pz)(CO_3)(H_2O)]_2(CF_3SO_3)_4{\cdot}2CH_3CN{\cdot}4H_2O$ (=$C_{62}H_{94}N_{22}O_{24}F_{12}S_4Cu_4$): C, 35.1 (34.8); H, 4.6 (4.4); N, 14.4 (14.4). ESI-MS, CH_3OH: *m/z*: z = 1, 1801 $[[Cu_2([22]pr4pz)(CO_3)]_2(CF_3SO_3)_3]^+$, z = 2, 827 $[[Cu_2([22]pr4pz)_2(CO_3)](CF_3SO_3)]^{2+}$.

$[Cu_2([22]pr4pz)(CH_3CN)_2](ClO_4)_2$ ($2(ClO_4)_2$): In a glove box, a solution of $[Cu(CH_3CN)_4]ClO_4$ (13.1 mg, 0.04 mmol) in 2 ml of dry methanol was added to a solution of [22]py4pz (9.8 mg, 0.02 mmol) in the same solvent. The diffusion of diethyl ether into the resulting solution led to the appearance of very small colorless crystals, suitable for X-ray diffraction analysis. The complex is easily oxidized and can only be stored in a dry glove box atmosphere. ^{1}H NMR (CD_3OD, 300 MHz, 25 ºC, TMS, ppm): δ = 7.72 (d, ^{3}J(H,H) = 2 Hz, 4H, 5'H-pz), 6.32 (d, ^{3}J(H,H) = 2 Hz, 4H, 4'H-pz), 4.87 (s, 8H, pz-(CH_2)$_2$-pz), 3.65 (s, 4H, N-CH_2-pz), 2.65 (t, ^{3}J(H,H) = 8 Hz, 4H, N-CH_2-C_2H_5), 1.50 (m, 4H, N-CH_2-CH_2-CH_3), 0.86 (t, ^{3}J(H,H) = 7 Hz, 6H, N-C_2H_5-CH_3) ppm. ESI-MS (CH_3CN) *m/z*: z = 1, $[[Cu_2([22]py4pz)]ClO_4]^+$ = 717.

8.4.3 Catecholase activity studies

The catecholase activity of $\mathbf{1}^{2+}$ was evaluated by reaction with 3,5-di-*tert*-butylcatechol at 25 ºC in methanol. The absorption at 400 nm (ε = 1400 $M^{-1}\cdot cm^{-1}$), characteristic of the formed quinone, was measured as a function of time. The experiments were run under a 1 atm of dioxygen. The kinetic parameters were determined for 2×10^{-5} M solutions of the complex (for simplicity, the complex concentration has been calculated based on the molecular weight of the dinuclear species $[Cu_2([22]pr4pz)(CO_3)(H_2O)](CF_3SO_3)_2\cdot CH_3CN\cdot 2H_2O$) and 0.05-3 mM solutions of the substrate. In a typical catalytic experiment, 2.5 ml of the solution of $\mathbf{1}^{2+}$ were placed in a 1 cm path-length cell, and the solution was saturated with dioxygen. Afterwards, 75 μl of the solution of substrate were added. After thorough shaking, the changes in UV-Vis spectra were recorded during 30 min.

8.4.4 Effect of dihydrogen peroxide on the kinetics of $DTBCH_2$ oxidation

The effect of dihydrogen peroxide on the reaction rates was studied in dioxygen-saturated methanol by varying the concentration of H_2O_2 in the range of 0.01–1 mM at constant concentrations of the complex (2×10^{-5} M) and $DTBCH_2$ (1 mM).

8.4.5 Effect of DTBQ on the kinetics of $DTBCH_2$ oxidation

The effect of DTBQ on the reaction rates was studied in dioxygen-saturated methanol by varying the concentration of DTBQ in the range of 0.01–0.412 mM at constant concentrations of the complex and $DTBCH_2$. The concentration of $\mathbf{1}^{2+}$ was 2×10^{-5} M, the concentration of $DTBCH_2$ 0.2 mM and 1 mM.

8.4.6 Detection of dihydrogen peroxide in the catalytic $DTBCH_2$ oxidation

The presence of dihydrogen peroxide in the reaction mixture was analyzed using the iodometric assay based on I_3^-, which has a characteristic absorption band at 353 nm (ε = 26000 $M^{-1}\cdot cm^{-1}$ in water). The oxidation reaction of $DTBCH_2$ by $\mathbf{1}^{2+}$ was carried out as described in the kinetic experiment. When the formation of quinone reached a desired value at 400 nm the solution was acidified with H_2SO_4 to pH 2 to stop the reaction. 3 ml of water was added and the reaction mixture was then extracted two times with CH_2Cl_2 to remove the formed DTBQ. To a 2 ml aliquot of the aqueous layer 1 ml of a KI solution (0.3 M) was added with a catalytic amount of lactoperoxidase to accelerate the formation of I_3^-. Blank experiments were performed under identical conditions in the presence of DTBQ and $\mathbf{1}^{2+}$, but only minor formation of I_3^- was observed.

8.4.7 X-ray crystallographic studies

X-ray intensities of $[H_2[22]pr4pz](ClO_4)_2$ were measured on Nonius KappaCCD diffractometer with rotating anode and graphite monochromator (λ = 0.71073 Å). The structure was solved with direct methods (SHELXS97[35]) and refined with SHELXL97[36] against F^2 of all reflections. $[C_{26}H_{40}N_{10}](ClO_4)_2$, Fw = 691.58, colorless/yellowish block (0.09×0.18×0.27 mm^3), monoclinic, space group *P2₁/c* (no. 14), a = 8.0611(14) Å, b = 11.660(2) Å, c = 17.306(3) Å, $\alpha = \gamma = 90°$, β = 96.557(16)°, V = 1615.9(5) $Å^3$, Z = 2, $\rho_{calc.}$ = 1.421 $g \cdot cm^{-3}$, μ = 0.264 mm^{-1}. A total of 23591 reflections, of which 3002 were independent [R(int) = 0.063], were collected in the range $2.1 \leq 2\theta \leq 25.5°$.Non-hydrogen atoms were refined freely with anisotropic displacement parameters. All hydrogen atoms were located in the difference Fourier map. The N-H hydrogen atom was refined freely with isotropic displacement parameters; C-H hydrogen atoms were refined with a riding model. Geometry calculations and checking for higher symmetry were performed with the PLATON package.[37]

X-ray intensities of compound $(\mathbf{1})_2(CF_3SO_3)_4 \cdot 2CH_3CN \cdot 4H_2O$ were measured on a Bruker AXS Apex diffractometer with a graphite monochromator. The structure was solved with direct methods (SHELXS97)[35] and the refinement was performed with SHELXL97[36] against F^2 of all reflections. Molecular illustrations, checking for higher symmetry and geometry calculations were performed with the PLATON package.[37] The entries for formula weight, density, F(000) and μ of complex are based on the formula $C_{54}H_{76}Cu_4N_{20}O_8(CF_3O_3S)_4 \cdot 2(C_2N) \cdot 4(O)$, which does not contain the hydrogen atoms of the solvent molecules. Fw = 2123.85, blue block (0.25×0.40×0.21 mm^3), monoclinic, space group *P21/n*, a = 18.716(5) Å, b = 15.043(5) Å, c = 32.110(5) Å, $\alpha = \gamma = 90°$, β = 103.118(5)°, V = 8804(4) $Å^3$, Z = 4, $\rho_{calc.}$ = 1.602 $g \cdot cm^{-3}$, μ = 1.156 mm^{-1}. A total of 25022 reflections, of which 8021 were independent [R(int) = 0.177], were collected in the range $1.3 \leq 2\theta \leq 25.9°$. The hydrogen atoms of the complex cation were calculated on idealized positions using a riding model with isotropic displacement parameters. The hydrogen atoms of the co-crystallized solvent molecules were not calculated. All non-hydrogen atoms were refined anisotropically. Final cycle refinement converged to R(F) = 0.0705 and *wR2* = 0.2007 (all reflections).

Due to sensitivity of $\mathbf{2}(ClO_4)_2$ towards dioxygen, the crystal was dropped into grease and then quickly frozen at 150 K on the Bruker AXS-Enraf-Nonius Kappa-CCD diffractometer using a graphite monochromator (λ (MoKα) : 0.71073Å). The crystal was twinned and the two components were separated using the EvalCCD software package with the following twin law [1 -0.65 -0.32, 0 -1 0, 0 0 -1] corresponding to a two fold axis along the [1 0 0] direction. The structure was solved by direct methods and refined by full matrix least-squares, based on F^2 from the HKLF5 file using the SHELXL97 software[36] through the WinGX program.[38] The fractional contributions of two domains were refined and are 0.737(1), 0.263(1). $[C_{30}H_{44}N_{12}Cu_2]Cl_2O_8$, Fw =

898.75, colorless block (0.50×0.32×0.16 mm^3), triclinic, space group $P\overline{1}$ (no. 2), a = 11.079(3) Å, b = 11.825(4) Å, c = 17.329(5) Å, α = 87.10(2)°, β = 74.92(2)°, γ = 68.81(2)°, V = 2041.5(11) $Å^3$, Z = 2, $\rho_{calc.}$ = 1.462 $g \cdot cm^{-3}$, μ = 1.233 mm^{-1}. A total of 38986 reflections, of which 10797 were independent, were collected in the range $1.22 \leq 2\theta \leq 30.11°$. All non-hydrogen atoms were refined with anisotropic thermal parameters. Hydrogen atoms were generated in idealized positions, riding on the carrier atoms, with isotropic thermal parameters. Final cycle refinement converged to $R(F)$ = 0.0591 and $wR2$ = 0.1632 (all reflections).

8.5 References

(1) Koval, I. A.; Belle, C.; Selmeczi, K.; Philouze, C.; Saint-Aman, E.; Schuitema, A. M.; Gamez, P.; Pierre, J.-L.; Reedijk, J. *J. Biol. Inorg. Chem.* **2005**, *10*, 739-750.
(2) Schuitema, A. M.; Aubel, P. G.; Koval, I. A.; Engelen, M.; Driessen, W. L.; Reedijk, J.; Lutz, M.; Spek, A. L. *Inorg. Chim. Acta* **2003**, *355*, 374-385.
(3) Schuitema, A. M. Ph.D. thesis, Leiden University, 2004.
(4) Addison, A. W.; Rao, T. N.; Reedijk, J.; van Rijn, J.; Verschoor, G. C. *J. Chem. Soc., Dalton Trans.* **1984**, 1349-1356.
(5) Chiari, B.; Piovesana, O.; Tarantelli, T.; Zanazzi, P. F. *Inorg. Chem.* **1993**, *32*, 4834-4838.
(6) van den Brenk, A. L.; Byriel, K. A.; Fairlie, D. P.; Gahan, L. R.; Hanson, G. R.; Hawkins, C. J.; Jones, A.; Kennard, C. H. L.; Moubaraki, B.; Murray, K. S. *Inorg. Chem.* **1994**, *33*, 3549-3557.
(7) van Albada, G. A.; Mutikainen, I.; Roubeau, O.; Turpeinen, U.; Reedijk, J. *Inorg. Chim. Acta* **2002**, *331*, 208-215.
(8) van Albada, G. A.; Mutikainen, I.; Roubeau, O. S.; Turpeinen, U.; Reedijk, J. *Eur. J. Inorg. Chem.* **2000**, 2179-2184.
(9) Chyn, J.-P.; Urbach, F. L. *Inorg. Chim. Acta* **1991**, *189*, 157-163.
(10) Kodera, M.; Kawata, T.; Kano, K.; Tachi, Y.; Itoh, S.; Kojo, S. *Bull. Chem. Soc. Jpn.* **2003**, *76*, 1957-1964.
(11) Balla, J.; Kiss, T.; Jameson, R. F. *Inorg. Chem.* **1992**, *31*, 58-62.
(12) Selmeczi, K.; Reglier, M.; Giorgi, M.; Speier, G. *Coord. Chem. Rev.* **2003**, *245*, 191-201.
(13) Eicken, C.; Krebs, B.; Sacchettini, J. C. *Curr. Opin. Struct. Biol.* **1999**, *9*, 677-683.
(14) Thompson, J. S.; Calabrese, J. C. *Inorg. Chem.* **1985**, *24*, 3167-3171.
(15) Benelli, C.; Dei, A.; Gatteschi, D.; Pardi, L. *Inorg. Chem.* **1990**, *29*, 3409-3415.
(16) Stallings, M. D.; Morrison, M. M.; Sawyer, D. T. *Inorg. Chem.* **1981**, *20*, 2655-2660.
(17) Klabunde, T.; Eicken, C.; Sacchettini, J. C.; Krebs, B. *Nat. Struct. Biol.* **1998**, *5*, 1084-1090.
(18) Thompson, J. S.; Calabrese, J. C. *J. Am. Chem. Soc.* **1986**, *108*, 1903-1907.
(19) Kaizer, J.; Pap, J.; Speier, G.; Parkanyi, L.; Korecz, L.; Rockenbauer, A. *J. Inorg. Biochem.* **2002**, *91*, 190-198.
(20) Neves, A.; Rossi, L. M.; Bortoluzzi, A. J.; Szpoganicz, B.; Wiezbicki, C.; Schwingel, E.; Haase, W.; Ostrovsky, S. *Inorg. Chem.* **2002**, *41*, 1788-1794.
(21) Monzani, E.; Quinti, L.; Perotti, A.; Casella, L.; Gulotti, M.; Randaccio, L.; Geremia, S.; Nardin, G.; Faleschini, P.; Tabbi, G. *Inorg. Chem.* **1998**, *37*, 553-562.
(22) Monzani, E.; Battaini, G.; Perotti, A.; Casella, L.; Gullotti, M.; Santagostini, L.; Nardin, G.; Randaccio, L.; Geremia, S.; Zanello, P.; Opromolla, G. *Inorg. Chem.* **1999**, *38*, 5359-5369.
(23) Karlin, K. D.; Gultneh, Y.; Nicholson, T.; Zubieta, J. *Inorg. Chem.* **1985**, *24*, 3725-3727.
(24) Plenge, T.; Dillinger, R.; Santagostini, L.; Casella, L.; Tuczek, F. *Z. Anorg. Allg. Chem.* **2003**, *629*, 2258-2265.
(25) Ackermann, J.; Meyer, F.; Kaifer, E.; Pritzkow, H. *Chem. Eur. J.* **2002**, *8*, 247-258.
(26) Börzel, H.; Comba, P.; Pritzkow, H. *Chem. Commun.* **2001**, 97-98.
(27) Torelli, S.; Belle, C.; Hamman, S.; Pierre, J. L.; Saint-Aman, E. *Inorg. Chem.* **2002**, *41*, 3983-3989.
(28) Koval, I. A.; van der Schilden, K.; Schuitema, A. M.; Gamez, P.; Belle, C.; Pierre, J.-L.; Luken, M.; Krebs, B.; Roubeau, O.; Reedijk, J. *Inorg. Chem.* **2005**, *44*, 4372-4382.
(29) Solomon, E. I.; Sundaram, U. M.; Machonkin, T. E. *Chem. Rev.* **1996**, *96*, 2563-2605.
(30) Monzani, E.; Casella, L.; Zoppellaro, G.; Gullotti, M.; Pagliarin, R.; Bonomo, R.; Tabbi, G.; Nardin, G.; Randaccio, L. *Inorg. Chim. Acta* **1998**, *282*, 180-192.

(31) Karlin, K. D.; Ghosh, P.; Cruse, R. W.; Meyer, G. J.; Farooq, A.; Gultneh, Y.; Jacobson, R. R.; Blackburn, N. J.; Strange, R. W.; Zubieta, J. *J. Am. Chem. Soc.* **1988**, *110*, 6769-6780.
(32) Paul, P. P.; Tyeklár, Z.; Jacobson, R. R.; Karlin, K. D. *J. Am. Chem. Soc.* **1991**, *113*, 5322-5332.
(33) Komarov, D. A.; Slepneva, I. A.; Glupov, V. V.; Khramtsov, V. V. *Free Radic. Res.* **2005**, *39*, 853-858.
(34) Slepneva, I. A.; Komarov, D. A.; Glupov, V. V.; Serebrov, V. V.; Khramtsov, V. V. *Biochem. Biophys. Res. Commun.* **2003**, *300*, 188-191.
(35) Sheldrick, G. M.; *SHELXS-97, Program for crystal structure solution*. University of Göttingen, Germany, 1997
(36) Sheldrick, G. M.; *SHELXL-97, Program for the refinement of crystal structures*. University of Göttingen, Germany, 1997
(37) Spek, A. L. *J. Appl. Cryst.* **2003**, *36*, 7-13.
(38) Farrugia, L. J. *J. Appl. Cryst.* **1999**, *32*, 837-838.